Available online at www.sciencedirect.com

SCIENCE DIRECT

Cement and Concrete Research 35 (2005) 1873 – 1881

Cement and Concrete Research

Rheological behavior of cement pastes from MRI velocimetry

S. Jarny[a,b], N. Roussel[b,*], S. Rodts[a], F. Bertrand[a], R. Le Roy[b], P. Coussot[a]

[a]*Laboratoire des Matériaux et des Structures du Génie Civil (LMSGC), Institut Navier, Champs sur Marne, France*
[b]*Laboratoire Central des Ponts et Chaussées (LCPC), Paris, France*

Received 6 April 2004; accepted 25 March 2005

Abstract

From MRI measurements, it is shown that in a flowing cement paste the thixotropic effects dominate over short time scales, while aging effects become significant over larger timescales. The steady state behavior, defined as flow properties in the intermediate period, exhibits a yielding behavior which differs from the prediction of usual yield stress models. The transition from the "solid" to the "liquid" regime is abrupt: the shear rate changes suddenly from zero to a finite value (critical shear rate) when the shear stress overcomes a critical value. These critical shear rates and shear stresses are independent of the flow conditions so that they may be considered as intrinsic material parameters. It was also shown that these results are consistent with usual macroscopic observations from conventional rheometry.

Keywords: Rheology; Magnetic Resonance Imaging; Physical properties; Cement paste

1. Introduction

Cement pastes are colloidal suspensions in which the particle interactions may lead to the formation of various microstructures. Depending on how such structures respond to an applied shear stress or strain rate, one observes different types of macroscopic flow behavior (Mewis and Spaull [1], Bird et al. [2], Coussot and Ancey [3]).The usual ways for describing steady state flow of fresh cement pastes involve Bingham, Herschel–Bulkley, Ellis, Casson or Eyring rheological models (Atzeni et al. [4]). In practice one determines macroscopic variables such as the torque and the rotation rate with a rotating geometry (Couette, parallel disks) and deduces the parameters of one of the above models. From a systematic comparison of these models in the case of Portland cement pastes Atzeni et al. [4] concluded that the Hershel Bulkley and Eyring models, which both involve a yield stress, appropriately represent the non-linear shear rate / shear stress curve of cement pastes. Yahia and Khayat [5] also studied the influence of the choice of one of the above models on the fitted yield stress value.

However these analyses concern steady state flows and it is worth noting that, for cement pastes, a relevant definition of steady state raises problems. As shown by Otsubo et al. [6], the flow properties of homogeneous fresh cement pastes continuously evolve in time. Under fixed boundary conditions (torque or rotation velocity) the apparent viscosity first decreases in time until reaching a minimum, then starts to increase. Banfill and Saunders [7] and Lapasin et al. [8] demonstrated that the first regime is dominated by a deflocculation phenomenon under constant shear rate (thixotropic behavior). Once this phenomenon has reached some equilibrium, the behavior keeps on evolving because of hydration process. This second effect is irreversible. Otsubo et al. associated the corresponding minimum shear stress at the transition between the two regimes to steady state and deduced the shear stress / shear rate (flow) curve.

This approach nevertheless neglects the possible strong heterogeneity of the shear rate distribution in non-Newtonian materials within rheometers. Indeed, for example in Couette flows with yield stress fluids, flow occurs only in a region close to inner cylinder where the local shear stress is larger than a critical value (the yield stress?). The thickness of this region decreases with the applied torque. This strong heterogeneity in the shear rate distribution can significantly

* Corresponding author.
E-mail address: Nicolas.roussel@lcpc.fr (N. Roussel).

0008-8846/$ - see front matter © 2005 Elsevier Ltd. All rights reserved.
doi:10.1016/j.cemconres.2005.03.009

affect the apparent behavior of the material since the *effective* (local) shear rate may widely differ from the *apparent* shear rate (relative velocity to gap ratio), and should be taken into account for comparison between theory and experiments. In order to avoid this heterogeneity, small gap Couette geometries are generally used. However, no matter how small the gap is, there will be an unsheared zone in the gap if the applied shear rate is sufficiently low, or when the applied shear stress approaches the yield stress. Moreover it is critical to know whether this shear localization is time-dependent or not, since this effect could be an additional source of time variations of the apparent viscosity (see the observations of Salmon et al. [9] for micellar solutions). The only way to deal with these phenomena consists to carry out measurements of local flow properties and interpret them in rheological terms, an approach which requires specific tools.

Here a rheological study of the behavior of cement pastes is undertaken using a Couette viscometer inserted in a Magnetic Resonance Imaging (MRI), hence making it possible to measure the local velocity field during transient and steady state flows. Since the local shear stress distribution is well controlled in such a Couette flow, the (measured) local shear rate can be associated to the local shear stress to deduce the effective (local) constitutive equation of the material. In the Second section the coupled MRI-rheometer set-up is described. Mix fitting and the preparation procedure of the tested cement paste along with usual rheometrical tests are described in the Third section. MRI-rheometry data are then presented and discussed in the Fourth section. In particular it is shown that the shear is strongly localized, which clearly proves the existence of a yield stress for such materials. However it is also demonstrated that classical yield stress models (Bingham, Herschel–Bulkley) are incapable of correctly representing the local behavior because, in contrast with the predictions of usual models, the effective solid–liquid transition is abrupt.

2. Proton NMR: a tool for velocity field measurement

Among many potential tools, proton Magnetic Resonance Imaging provides a powerful means to probe fluids dynamics. This technique is part of the Nuclear Magnetic Resonance (NMR) techniques, and uses magnetic properties of hydrogen nuclei (protons) in order to get spatially resolved physico-chemical or dynamic information inside a wide range of samples. These protons are often part of the fluid itself (e.g. water in our samples), and thereby, no tracers are required to perform measurements.

From a physical point of view, protons have a magnetic dipole moment which is sensitive to external magnetic fields. When these moments are placed into a strong magnetic field B_0, they exhibit a specific behavior which can be roughly described as threefold. First, moments naturally tend to get to some equilibrium position aligned along B_0. Secondly, if those moments are 'pushed away' from this position, they do not just simply come back along B_0, but start instead to precess together around B_0, at the rate of the so-called Larmor frequency:

$$\omega_0 = \gamma B_0 \tag{1}$$

where γ is the gyromagnetic ratio of protons. This precession motion eventually loses amplitude and the moments progressively come back to their equilibrium state along B_0. Finally, the kinetics of this last process are characterised by a 'relaxation time' of the NMR signal which depends on the properties of the sample being tested.

In any NMR facility, a magnet creates a strong homogeneous magnetic field inside the sample. A radio-frequency antenna is used to push the protons out of equilibrium, and provide instantaneous measurements of the amplitude and phase of precession movements. For the purpose of density imaging and motion detection, one additionally uses field gradients generated at will by specific coils surrounding the sample. When such a gradient is applied, the local Larmor frequency in the sample becomes a linear function of spatial position:

$$\omega(r) = \gamma(B_0 + G{\cdot}r) \tag{2}$$

Let us consider a fluid element in 'magnetic precession', initially situated in r and moving with a (slowly varying) velocity $\vec{v}$, and which undergoes a gradient $G(t)$ during a short time interval $[0,T]$. It may be shown that, after a time T, the precession movement of protons inside the fluid element will only be affected–as compared to precession under the homogeneous B_0 field–by a phase shift:

$$\Delta\phi = k_1{\cdot}\vec{r} + k_2{\cdot}\ \vec{v} \qquad \text{with } k_1 = \gamma\int_0^T G(t)dt$$
$$\text{and } k_2 = \gamma\int_0^T G(t)tdt \tag{3}$$

$\Delta\phi$ thus provides (indirect) information about the location and velocity of the fluid. In slowly varying flows, measurements of this phase shift during successive periods of proton precession while varying k_1 and k_2 values in a systematic way allows, through specific data processing procedures, to obtain the velocity field anywhere in the sample.

In the present study, proton NMR velocity measurements were carried out with a Bruker Biospec 24/80 DBX imager located at LMSGC. It is equipped with a 0.5 T vertical magnet (20 MHz proton frequency, diameter: 40 cm), with shielded gradient coils delivering a gradient of 50 mT/m, and with a linear birdcage RF coil of 24 cm length and 20 cm inner diameter (Fig. 1). For the purpose of such coupled MRI-rheometry experiments, a custom built Couette rheometer was used, specifically designed to comply with MRI constraints. The relatively large size of samples it can accept makes it suitable for studying civil engineering materials

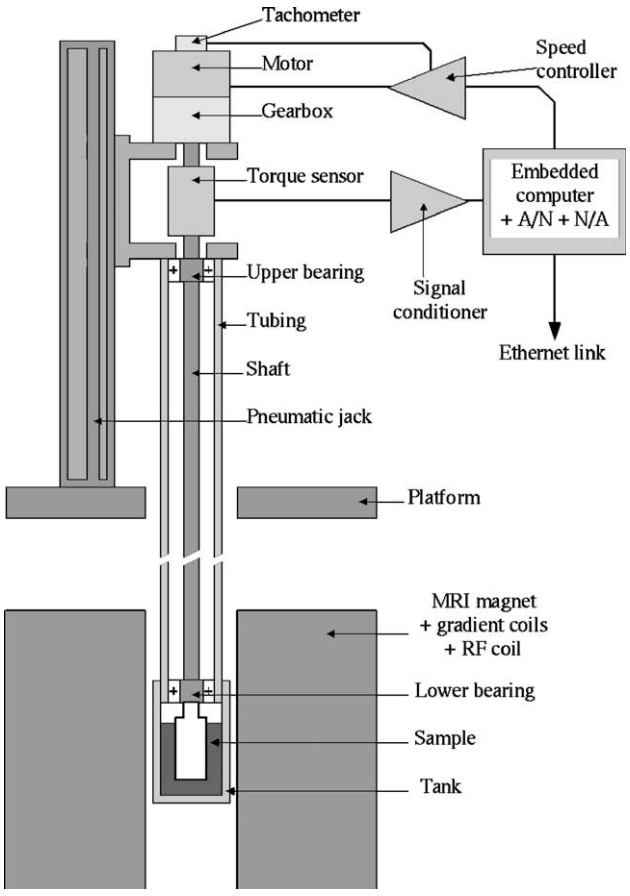

Fig. 1. Schematic representation of the MRI-rheometer [11].

containing coarse particles (cement, concrete, muds, granular pastes, etc.). All the parts of the apparatus inserted in the magnet were built with non-magnetic materials and the motor was moved as far as possible from the magnet entrance. A coaxial cylinder viscometer (inner cylinder: $r_1 = 40.7$ mm (radius), length: $h = 113.5$ mm) was used with a fix outer cylinder (radius $r_2 = 59.3$ mm) as shown in Fig. 2. The surfaces of the outer and inner cylinder in contact with the fluid were covered with sandpaper with an equivalent roughness of 200 μm. In contrast with most previous works in the MRI field this rheometer is vertical, like usual laboratory rheometers. The rotating axis lies on two bearings situated at its two extremities. The entire system is set up on a pneumatic jack: its lowest position places the cylinder out of the magnet so that the tools or the samples can easily be removed or set up, while its highest position is such that the shear geometry is at the magnet center. The samples can also be set up during axis rotation so that the time interval between the end of hand mixing and preshear is short. The imposed rotation velocity Ω can be varied over a wide range (from 0.002 to 1000 rpm) by adding a reducer after the direct current (dc) motor. This rheometer is remotely controlled via a computer and the velocity can be imposed step by step or in (almost) continuous ramps. The temperature of the material in the Couette geometry could not be controlled but the room temperature was maintained between 20 and 24 °C.

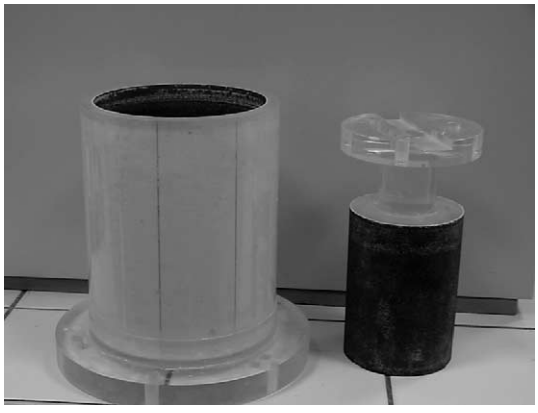

Fig. 2. Modified rough inner and outer cylinders of the MRI-rheometer.

MRI velocity measurements inside the Couette cell were obtained according to the method first introduced by Hanlon et al. [10] and further modified by Raynaud et al. [11]. The NMR sequence is depicted in Fig. 3. Two successive RF emissions coupled with field gradients labelled (a) and (b) respectively select in the y and z directions a virtual beam along one diameter of the Couette cell (Fig. 4(a) and (b)). The pair of gradients (in black) in the y direction introduces in the local NMR signal a strong phase shift proportional to the ortho-radial velocity inside the flow. Field gradients applied in the x direction (c) allow detailed spatial information about the NMR signal along the beam at the time of signal measurement to be collected (d).

Comparison of two different measurements obtained for two different strengths of velocity encoding gradients makes it possible to remove spurious phase shifts in the NMR signal, and eventually to get the 'pure' velocity phase shift along the x direction. Further simple numerical treatment then provides the velocity field.

One major difficulty with MRI measurements on cement paste is the very low value of the so-called T_2 relaxation time of water (about 4 ms). Given that a few milliseconds are also necessary to carry out one NMR sequence, such a short value leads to a very weak signal to noise ratio at the time of signal acquisition. However, this difficulty can be overcome by specific tuning of the NMR sequence and data processing (Rodts et al. [12]), and correct velocity profiles can be obtained in an experimental time as short as 5 s. The

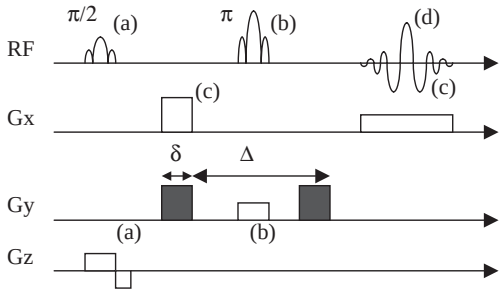

Fig. 3. MRI velocimetry sequence.

(a)

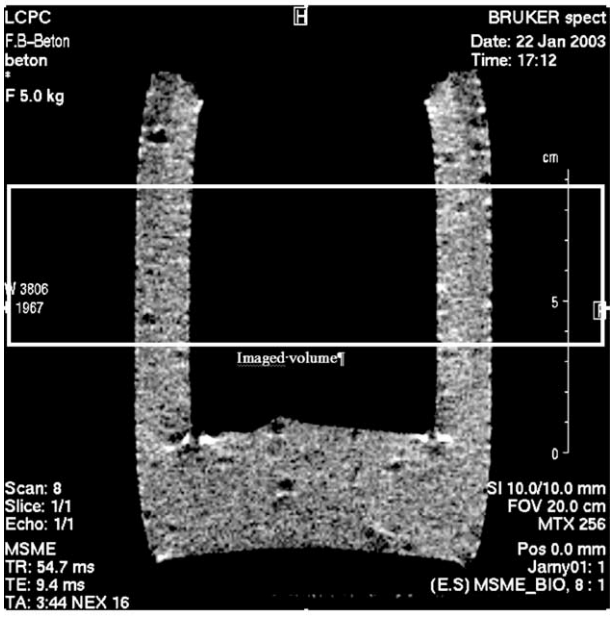

(b)

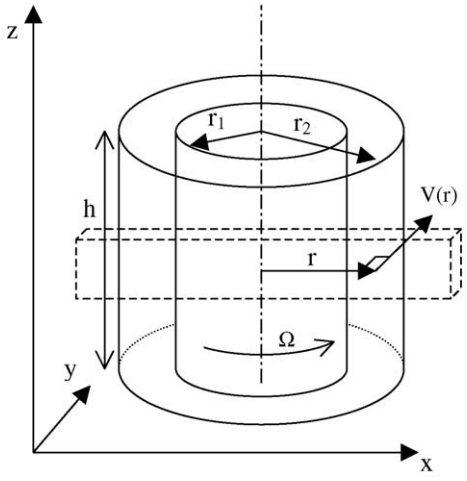

Fig. 4. Views of the imaged volume: from NMR density imaging in a longitudinal section (a), from a 3D representation (b). The white frame in (a) corresponds to the parallelepiped drawn in (b).

spatial resolution of our measurements is 0.5 mm. The uncertainty in velocity data was estimated theoretically from the amplitude of electromagnetic and electronic noise. It was typically of the order of 1 mm/s, but since it also depends on the velocity and position, error bars are included in Fig. 7.

3. Material and procedures

3.1. Mix design

In order to minimize C4AF amount in the material, white cement was chosen, as Fe paramagnetic oxides enhance relaxation kinetic, thus leading to very poor signal to noise ratio. As the cement particles had to be stable for at least 1 h (neither static sedimentation nor dynamic segregation during testing) a viscosity agent was added. After a series of preliminary (rheometrical) tests with different materials, the mix design given in Table 1 was chosen as it provided a cement paste with a rheological behavior representative of the various batches tested, i.e. yield stress and shear thinning behavior, obvious structuration at rest and time dependency as observed by other authors [13]. The W/C of our cement paste was 0.35.

Table 1
Cement paste composition

Component	Mass [g]
White cement CEM I 52,5 Calcia《Cruas》	2000
Superplasticizer optima 100 Chryso	46.7
Nano silica Rhoximat Rhodia	177
Distilled water	530.3

3.2. Preparation procedure

The superplasticiser was introduced in the mixing water and the solution obtained was mixed at 260 rpm for 60 s. The white cement and the nanosilica particles were then added. The suspension obtained was mixed at 700 rpm for 15 min and then at 260 rpm for 15 min. This (long) mixing aims to give the superplasticiser enough time to play its full role in the mixture and disperse the cement particles. The end of preparation corresponds to time T_0.

3.3. Rheometry

Conventional rheometrical tests were carried out during the first hour following mixing at T_0+2 min,

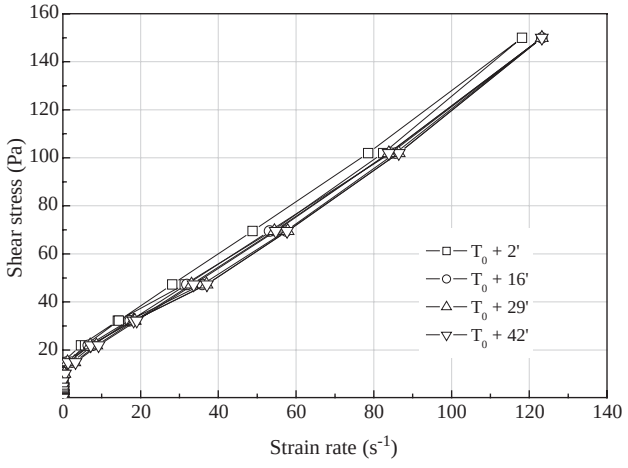

Fig. 5. Flow curve of the cement paste at different time intervals following preparation determined by conventional rheometry (see text).

T_0+16 min, T_0+29 min and T_0+42 min (Fig. 5), with a HAAKE ViscoTester® VT550. The inner cylinder and outer cylinder radii r_1 and r_2 were respectively 18.9 and 21.0 mm. The inner cylinder height h was 56.5 mm. Before each measurement, a pre-shear at 150 s^{-1} was applied to each sample. Then the apparent shear rate was increased step by step from 0.5 s^{-1} to 120 s^{-1}. The shear rate was changed to the next level either because the measured torque C appeared stabilized or because the maximum step duration (30 s) was reached. The set of apparent shear rate $\dot{\gamma}=\Omega r_1/(r_2-r_1)$ and corresponding apparent shear stress $\tau=C/2\pi hr_1^2$ [2] gave the apparent flow curve of the material (cf. Fig. 5). Herschel–Bulkley and Bingham models were fitted to the flow curve obtained at T_0+17 min. The corresponding parameters are τ_0=14 Pa, n=0.93, K=1.5 SI (Herschel–Bulkley) and τ_0=15 Pa and η=1.1 Pa s (Bingham).

4. MRI results

4.1. Testing procedure

After a 2 min preshear at 134 rpm, the rotating speed was immediately switched down to a fixed value between 10.3 and 103.1 rpm at which it was left during half an hour. Throughout the test, the velocity field was determined every 10 s. A new sample was prepared before each test under new rotating speed.

4.2. Steady state experimental results

A typical set of fluid velocity variations with time at different distances from the axis under a given rotating speed of the inner cylinder is shown in Fig. 6. In a first stage there is a relatively rapid evolution of the velocity: close to the inner cylinder it slightly decreases, further from the inner cylinder the velocity strongly decreases until apparent stoppage at the critical radius beyond which no velocity was recorded from the initial time. Beyond about 100 s of flow the velocity starts to increase at a greater rate for larger distances. Note that before any further analysis (see Section 4.5) of this data we have no information about the local viscosity. However these trends concerning the velocity field can naturally be put in qualitative correspondence with the evolutions of viscosity and internal structure of cement pastes with time as described by Otsubo et al. [6] and Banfill and Saunders [7]. In this context, the following interpretation is suggested: over short timescales (first stage) flocculation and deflocculation processes dominate, which lead to rapid thixotropic (reversible) effects, while over larger timescales hydration processes dominate, which lead to irreversible evolutions of the local behavior of the fluid. These two effects might in fact act at any time but according to the above scheme they appear to have very different characteristic times. As a consequence it is reasonable to consider that there exists an intermediate period, say around 100 s, for which reversible effects have become negligible whereas irreversible effects have not yet become significant. This period corresponds to what we will define as the "steady state" flow regime of the material.

The steady state velocity profiles under different rotation velocities (Ω) of the inner cylinder are shown in Fig. 7. Note first that, for each level, the velocity extrapolated from these data towards the inner radius almost exactly corresponds to the tangential velocity (Ωr_1) along the rotating cylinder, which indicates that wall slip was negligible. This is not necessarily in contradiction with previous results [14,15]: indeed here we simply observed that the velocity difference between the material and the tool is negligible compared to the material velocity in this region, but this difference might

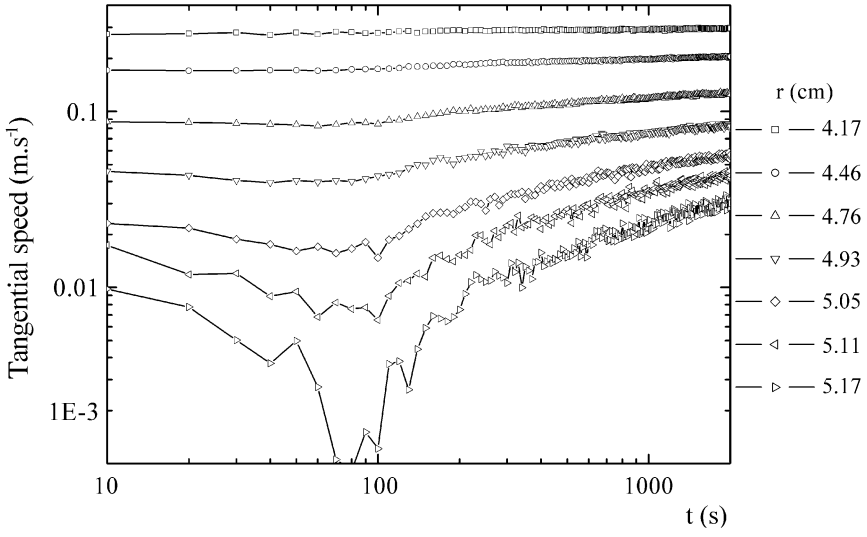

Fig. 6. Tangential velocity as a function of time at different radii inside the gap. A point of measure is obtained each 10 s. The apparent velocity for distances larger than 5.17 cm was zero within the uncertainty on our measurements. Inner cylinder rotating speed: 82.4 rpm.

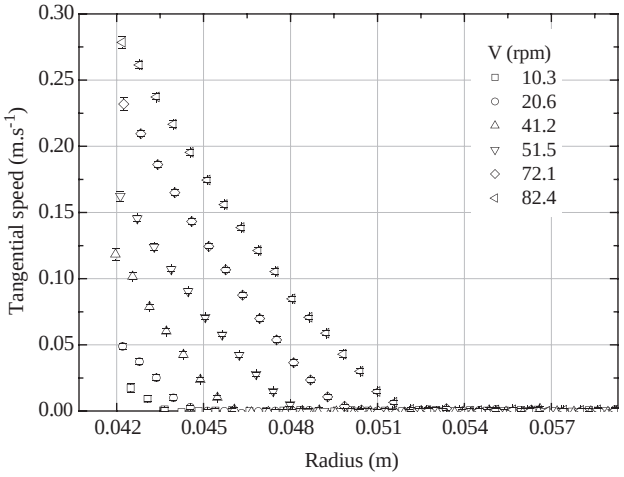

Fig. 7. Steady state tangential velocity as a function of radius inside the gap for several inner cylinder rotating speeds after 100 s of flow. Error bars for each measurements are also plotted.

become significant under lower rotation velocities, i.e. when the fluid velocity is significantly lower.

The velocity profiles exhibit two distinct regions: close to the inner cylinder the paste is sheared and the velocity decreases almost linearly as a function of the distance. In the second region the paste apparently does not flow. The interface between these two regions is situated at a critical distance r_c, which increases with the rotation speed of the inner cylinder: the thickness of the sheared region increases with Ω. It is worth noting that the transition between these two regions seems somewhat abrupt in terms of shear rate: the slope of the velocity profile abruptly turns from a finite, constant slope to almost zero, a phenomenon already observed with other thixotropic materials such as bentonite suspensions [16,17]. Although this effect seems to be intimately linked to the behavior of the homogeneous paste in the case of bentonite suspensions it is not so clear for cement pastes in which the largest solid particles might migrate through the interstitial liquid during flow. In the following section, we present data which demonstrate that such migrations effects are negligible within the duration of our tests, and that the observed trends reflect the behavior of the homogeneous cement paste. It is worth noting that the first velocity profile, measured after 10 s of flow, already exhibits distinct sheared and unsheared regions with a slope break at the interface. Since within such a duration a significant migration could hardly have time to develop, this already suggests that, under the experimental conditions used, this shear localization basically corresponds to an abrupt behavior transition controlled by stress or strain and not by density change.

4.3. Water content MRI measurements

The time variations and the steady state aspects of our velocity profiles might partly reflect migration or segregation effects during flow. In particular the farthest regions could contain a higher concentration of particles and thus have a higher viscosity, which could contribute to the shear localisation. In this context it is necessary to check that the samples remained homogeneous during the tests. In this aim standard relaxation weighted density imaging was carried out.

In order to check the sensitivity of the imaging technique to particle concentration, we first imaged a series of homogeneous cement pastes with different water contents in containers at rest (W/C=0.33, 0.35, 0.37 respectively). With this technique the average grey levels in the images mostly reflect the local density and relaxation time of protons from a qualitative point of view. Local grey scale heterogeneities which can be seen inside each sample should be regarded here as imaging artefacts, and are a priori due to both local magnetic susceptibility heterogeneities originating from possible small air bubbles, and poor signal to noise ratio. Thus, in the following analysis, only the average grey level at a slightly larger scale than that of heterogeneities is considered. Above W/C=0.35, significantly different grey levels appear for W/C differences as low as 0.02 (Fig. 8), which implies that standard NMR imaging is capable to identifying smaller water content increase within a single sample. Taking advantage of this result it can be concluded that no heterogeneity in W/C larger than say 0.01 developed in the sample during flow since the average grey level appears homogeneous in the gap at the end of a flow test (Fig. 9).

4.4. Analysis in terms of a simple yield stress model

As a first approximation, yield stress models predict a shear localization as observed here, so that it is natural to expect that a (simple) yield stress model can be fitted to the data in steady state. Indeed all these models predict that no

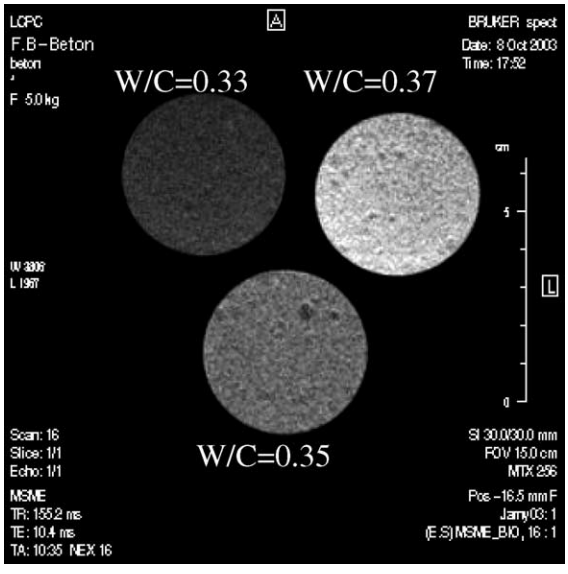

Fig. 8. NMR density images in a horizontal cross-section of the containers, of homogeneous cement pastes of different water contents (W/C).

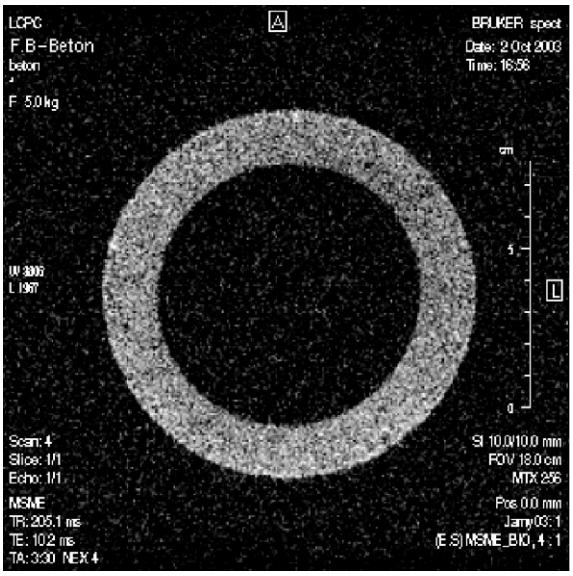

Fig. 9. NMR density imaging, in a horizontal cross-section of the Couette cylinder, of the cement paste just after flow.

flow should occur beyond a critical distance at which the shear stress equals the yield stress. The predictions of the models (here we focus on the Bingham and Herschel–Bulkley models) in terms of velocity within a Couette flow can be determined numerically (analytical solutions only exist for integer values of the power coefficient and in particular for a Bingham model) from the integration of the momentum and constitutive equations. These predictions can be compared to the experimental profiles by fitting of parameters. It appears that the measured velocity profiles are fundamentally different from those expected for fluids following such ideal yield stress models. Indeed, at any scale of observation, these models predict a continuous transition from sheared to unsheared region, i.e. the shear rate, and thus the slope of the velocity profile, continuously tends to zero at the approach of the interface between the sheared and the unsheared regions [17]. In practice this means that it is not possible to find rheological parameters which would fit the measured local velocity under three criteria (Fig. 10).

With the Bingham model, the values obtained for the plastic viscosity differ from those determined from conventional rheometry (see Section 3.3 and Fig. 5). Moreover, the shapes of the theoretical and experimental velocity profiles significantly differ whatever the rheological parameters. With the Herschel–Bulkley model, the constitutive equation obtained when one tries to have the same unsheared thickness corresponds to shear-thickening ($n>1$), which is in major disagreement with the results from conventional rheometry (cf. Section 3.3). With the other criteria (see Fig. 10) the rheological parameters are in good agreement with those of the usual approach (cf. Section 3.3). However, it remains impossible to find a set of τ_0, n and K parameters such that the velocity profile fulfils our three basic criteria. To compare the values of the parameters, it is necessary to check that the same range of shear rates is studied in both approaches. The range of apparent shear rates is [1 s^{-1}; 120 s^{-1}] for the conventional rheometry results (see Fig. 5) and the range of local shear rates is [10 s^{-1}; 50 s^{-1}] for the MRI results. (for more details about the calculus of the shear rate from velocity measurements see Section 4.5). These ranges are close enough for the comparison to be valid.

4.5. Further analysis of the velocity profiles

The slope of the velocity profile is related to the shear rate via $\dot{\gamma}=r\partial(V/r)/\partial r=\partial V/\partial r - V/r$ [2], in which $V(r)$ is the local velocity at the distance r. Since along the interface, i.e. at $r=r_c$, we have $V(r)=0$, the critical shear rate is equal to the slope of the velocity profile:

$$\dot{\gamma}_c = \dot{\gamma}(r_c) = \left(\frac{\partial V}{\partial r}\right)_{r_c} \quad (4)$$

Despite some slight fluctuations which may be due to experimental uncertainties inherent to this type of material this critical shear rate appears (Fig. 11) independent of the flow conditions (rotation velocities of the inner cylinder),

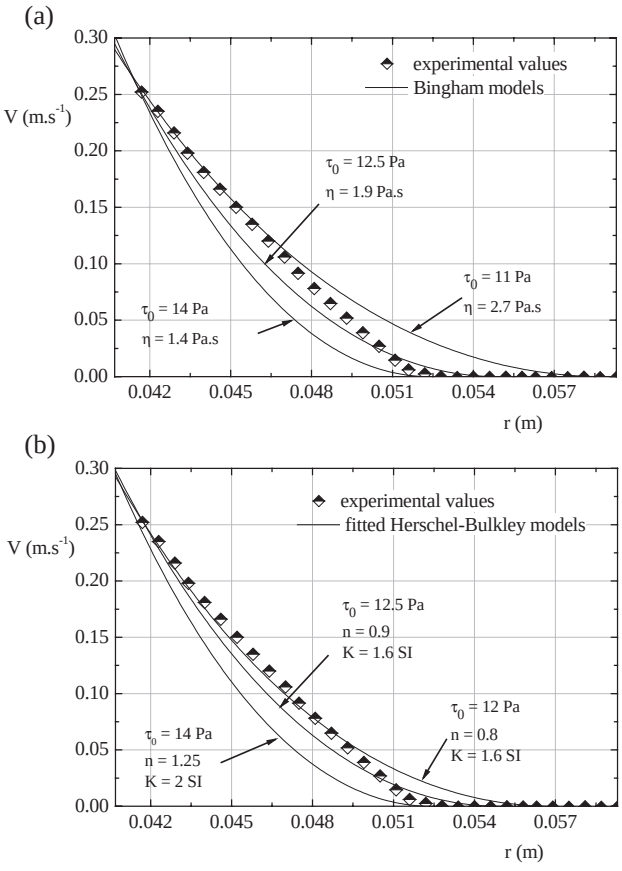

Fig. 10. Velocity as a function of distance within the gap of a Couette flow for a 72.1 rpm rotating speed after 100 s. Continuous lines correspond to the predictions using various best fits of the Bingham (a) and Herschel–Bulkley model (b) with different conditions: same unsheared thickness, similar slope in the sheared region, same overall shape.

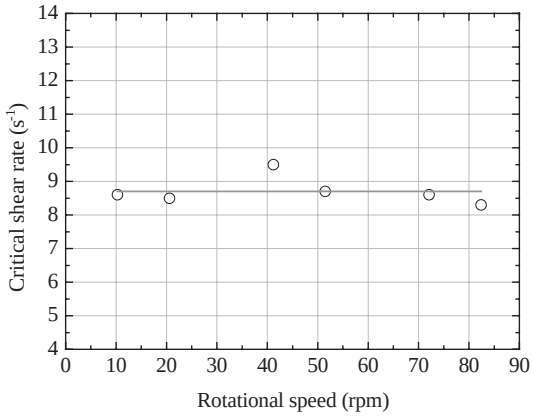

Fig. 11. Critical shear rate in the velocity profiles of Fig. 7. The continuous line corresponds to the average level.

which suggests that this is an intrinsic rheological parameter of the fluid. Its average value is 8.7 s^{-1} for the cement paste tested.

The shear stress distribution simply results from the momentum balance: $\tau = C/2\pi hr^2$ [2], in which C is the torque applied to the inner cylinder and h the height of sheared fluid. As a consequence the critical stress associated with the interface between the sheared and unsheared regions expresses as:

$$\tau_c = \frac{C}{2\pi r_c^2 h} \tag{5}$$

Here again the corresponding experimental values appear (Fig. 12) to slightly vary around a constant, average value (here 14 Pa), which suggests that this critical stress is also an intrisic, rheological parameter of the fluid, associated to the critical shear rate.

Thus the effective rheological behavior of our material differs from the simple yielding behavior assumed through usual yield stress models: the material cannot flow in steady state below a critical shear stress τ_c; beyond τ_c it flows at a shear rate larger than $\dot{\gamma}_c$; one cannot obtain stable flows under (effective) shear rate in the range $[0; \dot{\gamma}_c]$. This in particular explains why the velocity distribution in Couette flows cannot be represented by a Bingham or a Herschel–Bulkley models.

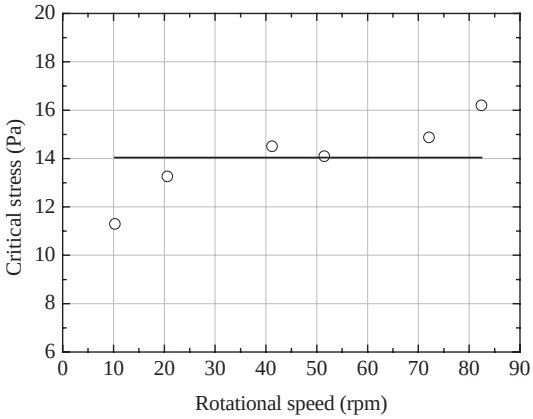

Fig. 12. Critical shear stress in the velocity profiles of Fig. 7. The average critical shear stress value is plotted in solid line.

At first sight these results might appear inconsistent with all previous (macroscopic) measurements concerning cement pastes but in fact this is not the case. First the data show that cement paste exhibits a *yield stress* below which no stable flow occurs and the value of which is close to the values found by fitting the usual yield stress models to conventional rheometrical data (this paragraph and Section 3.3). Secondly the effective rheological behavior of the material implies that, as the shear stress along the inner cylinder (usually considered as the apparent shear stress) decreases to the critical stress, the thickness $(r_c - r_1)$ of the sheared region decreases to zero while the (effective) shear rate in this region tends to $\dot{\gamma}_c$. The rotation velocity thus becomes $\Omega \approx \dot{\gamma}_c(r_c - r_1)/r_1$. This implies that the apparent shear rate, i.e. $\Omega r_1/(r_2 - r_1) \approx \dot{\gamma}_c(r_c - r_1)/(r_2 - r_1)$, tends continuously to zero as the shear stress tends to the critical stress. This means that the apparent flow curve as deduced from macroscopic measurements from conventional techniques should correspond to that of a simple yield stress model even if the effective behavior is as observed here. In particular the yield stresses obtained from both approaches are similar.

The results presented here do not completely contradict previous interpretations of rheological measurements but provide explanations of some peculiar effects. For example it may be observed that cement pastes tend to stop flowing rather abruptly when poured over a solid surface. This is not explained by simple yield stress models which predict that the flow rate should progressively decrease (typically over one to several hours for the flow of a given amount of material over an inclined plane [18]) as the fluid spreads and the maximum value of the second stress invariant decreases towards the yield stress. However, this finds a natural

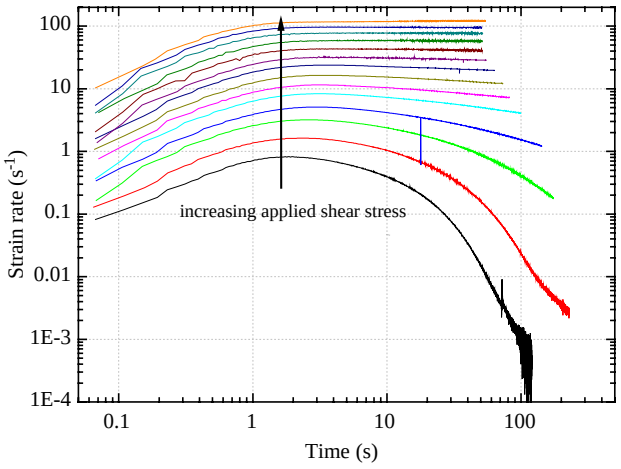

Fig. 13. Apparent shear rate vs. time for the cement paste under different imposed shear stress values from 0.5 to 100 Pa. (stress levels from bottom to top: 0.5, 1, 2, 3, 5, 7, 10, 15, 20, 30, 40, 60, 80 and 100 Pa).

explanation from our results: the fluid first spreads relatively rapidly at a rate larger than a critical, finite value, but when the second stress invariant reaches the yield stress the flow becomes unstable and abruptly stops. This phenomenon may be directly observed from conventional rheometrical creep tests with the cement paste (Fig. 13).

The apparent shear rate in time evolves differently depending on the value of the imposed stress. For an applied shear stress below the critical shear stress, the flow rapidly stops. For an applied shear stress higher than the critical shear stress, the inner cylinder keeps on rotating at an almost constant value. In this case the lower the applied shear stress, the longer is the time needed for flow to stop. Note the very similar aspect of this set of shear rate vs. time curves and the set of local velocities vs. time at different distances (and thus different stresses) in the Couette system under a given rotation velocity during the first 100 s (Fig. 6). This similarity proves the qualitative consistency of macroscopic and local data.

Our results also suggests an explanation to some peculiar effects observed at low apparent shear rates (flow curve with a minimum [19]). Indeed in that case the sheared thickness is very small and can become equal to a few particle diameters. In this region the continuum assumption is no longer valid, the material flows in a "discrete" regime in which it a priori has no intrinsic rheological behavior. Under these conditions the apparent flow curve may decrease or increase, depending on the size of the sheared thickness and the specific local arrangements of the particles in this small thickness.

5. Conclusion

From MRI measurements, it can be shown that cement paste exhibits a yielding behavior which differs from the prediction from of usual models: the transition from the solid (below τ_c) to the liquid regime (above τ_c) is abrupt, i.e. the shear rate changes suddenly from zero to a finite value $\dot{\gamma}_c$ when the shear stress overcomes τ_c. It has also been shown that these results are consistent with usual macroscopic observations. Since in addition this cement paste has been chosen because its apparent mechanical behavior was representative of that of a large range of cement pastes it is likely that those conclusions can apply to most cement pastes.

The focus of this study was steady state properties, but time effects were also identified (Figs. 6 and 13). The next step will be to further analyze these transient effects at a local scale and interpret them in terms of a thixotropic model. This model should represent the effective behavior more accurately than models deduced from macroscopic data which cannot take into account spatial heterogeneities of the viscosity.

Acknowledgements

The Laboratoire des Matériaux et des Structures du Génie Civil is a research unity (N°113) associated to Laboratoire Central des Ponts et Chaussées, Ecole des Ponts et Chaussées and Centre National de la Recherche Scientifique.

References

[1] J. Mewis, A.J.B. Spaull, Rheology of concentrated dispersions, Adv. Colloid Interface Sci. 6 (1976) 173–200.
[2] R.B. Bird, D. Gance, B.J. Yarusso, The rheology and flow of viscoplastic materials, Rev. Chem. Eng. 1 (1982) 1–70.
[3] P. Coussot, C. Ancey, Rheophysical classification of concentrated suspensions and granular paste, Phys. Rev. Lett. E 59 (1999) 4445–4457.
[4] C. Atzeni, L. Massidda, U. Sanna, Comparison between rheological models for Portland cement pastes, Cem. Concr. Res. 15 (1985) 511–519.
[5] A. Yahia, K.H. Khayat, Analytical models for estimating yield stress of high performance pseudo-plastic grout, Cem. Concr. Res. 31 (2001) 731–738.
[6] Y. Otsubo, S. Miyai, K. Umeya, Time-dependent flow of cement pastes, Cem. Concr. Res. 10 (1980) 631–638.
[7] P.F.G. Banfill, D.C. Saunders, On the viscometric examination of cement pastes, Cem. Concr. Res. 11 (1981) 363–370.
[8] R. Lapasin, A. Papo, S. Rajgelj, Flow behaviour of cement pastes. A comparison of different rheological instruments and techniques, Cem. Concr. Res. 13 (1983) 349–356.
[9] J.B. Salmon, S. Manneville, A. Colin, Shear-banding in a lyotropic lamellar phase: Part I. Time-averaged velocity profiles, Phys. Rev., E Stat. Phys. Plasmas Fluids Relat. Interdiscip. Topics 68 (2003) 51503.
[10] A.D. Hanlon, S.J. Gibbs, L.D. Hall, D.E. Haycock, W.J. Frith, S. Ablett, Rapid MRI and velocimetry of cylindrical Couette flow, Magn. Reson. Imaging 16 (8) (1998) 953–961.
[11] J.S. Raynaud, P. Moucheront, J.C. Baudez, F. Bertrand, J.P. Guilbaud, P. Coussot, Direct determination by NMR of the thixotropic and yielding behavior of suspensions, J. Rheol. 46 (2002) 709–732.
[12] S. Rodts, F. Bertrand, S. Jarny, P. Poullain, P. Moucheront, Recent developments in MRI applications to rheology and fluid mechanics (in French), C R Chimie 7 (2004) 275–282.
[13] R. Shaughnessy, P.E. Clark, The rheological behaviour of fresh cement pastes, Cem. Concr. Res. 18 (1988) 327–341.
[14] A.W. Saak, H.M. Jennings, S.P. Shah, The influence of wall slip on yield tress and viscoelastic measurements of cement pastes, Cem. Concr. Res. 31 (2001) 205–212.
[15] M. Nehdi, M.-A. Rahman, Estimating rheological properties of cement pastes using various rheological models for different test geometry, gap and surface friction, Cem Conc Res, (in press) (Uncorrected proof available online).
[16] P. Coussot, Q.D. Nguyen, H.T. Huynh, D. Bonn, Viscosity bifurcation in thixotropic, yielding fluids, J. Rheol. 46 (3) (2002) 573–589.
[17] N. Roussel, R. Le Roy, P. Coussot, Test of a thixotropy model by comparison with local and macroscopic flow properties, J. Non-Newton. Fluid Mech. 117 85–95.
[18] S. Jarny, P. Coussot, Characterization of paste flows in a Couette geometry, Rhéologie 2 (2002) 52–63 (in French).
[19] P. Coussot, S. Boyer, Determination of yield stress fluid behaviour from inclined plane test, Rheol. Acta 34 (1995) 534–543.